Complex	Docking Score / kJmol-1
Cas13a-crRNA-1	-1892.39
Cas13a-crRNA-2	-1803.78
Cas13a-crRNA-3	-1696.54
Cas13a-crRNA-4	-1854.38
Cas13a-crRNA-5	-1850.75
Cas13a-crRNA-6	-1836.12
Cas13a-crRNA-7	-1810.80
Cas13a-crRNA-8	-1886.41
Cas13a-crRNA-9	-1885.52
Cas13a-crRNA-10	-2005.76
Cas13a-crRNA-11	-1771.68
Cas13a-crRNA-12	-1846.63
Cas13a-crRNA-13	-1687.46
Cas13a-crRNA-14	-2023.14
Cas13a-crRNA-15	-1778.41
Cas13a-crRNA-16	-1828.01
Cas13a-crRNA-17	-1915.44
Cas13a-crRNA-18	-1812.40
Cas13a-crRNA-19	-1855.09
Cas13a-crRNA-20	-1877.78
Cas13a-crRNA-21	-1760.50
Cas13a-crRNA-22	-1971.52
Cas13a-crRNA-23	-1804.31
Cas13a-crRNA-24	-1844.74
Cas13a-crRNA-25	-1685.98
Cas13a-crRNA-26	-1879.68
Cas13a-crRNA-27	-1820.65
Cas13a-crRNA-28	-1694.57

Cas13a-crRNA-29	-1875.07

Table S1 Molecular docking results of single-stranded crRNA with Cas13a

Complex	Docking Score / kJmol-1
Cas13a-RNA1	-2288.28
Cas13a-RNA2	-2200.71
Cas13a-RNA3	-2326.04
Cas13a-RNA4	-2349.62
Cas13a-RNA5	-2334.89
Cas13a-RNA6	-2436.99
Cas13a-RNA7	-2182.40
Cas13a-RNA8	-2318.55
Cas13a-RNA9	-2458.62
Cas13a-RNA10	-2529.97
Cas13a-RNA11	-2416.96
Cas13a-RNA12	-2440.35
Cas13a-RNA13	-2023.00
Cas13a-RNA14	-2512.49
Cas13a-RNA15	-2261.23
Cas13a-RNA16	-2290.57
Cas13a-RNA17	-2365.03
Cas13a-RNA18	-2424.13
Cas13a-RNA19	-2209.53
Cas13a-RNA20	-2363.88
Cas13a-RNA21	-2239.78
Cas13a-RNA22	-2533.62
Cas13a-RNA23	-2396.80
Cas13a-RNA24	-2300.80

Cas13a-RNA25	-2422.91
Cas13a-RNA26	-2354.48
Cas13a-RNA27	-2452.40
Cas13a-RNA28	-2441.87
Cas13a-RNA29	-2205.07

Table S2 Molecular docking results of double-stranded RNA with Cas13a

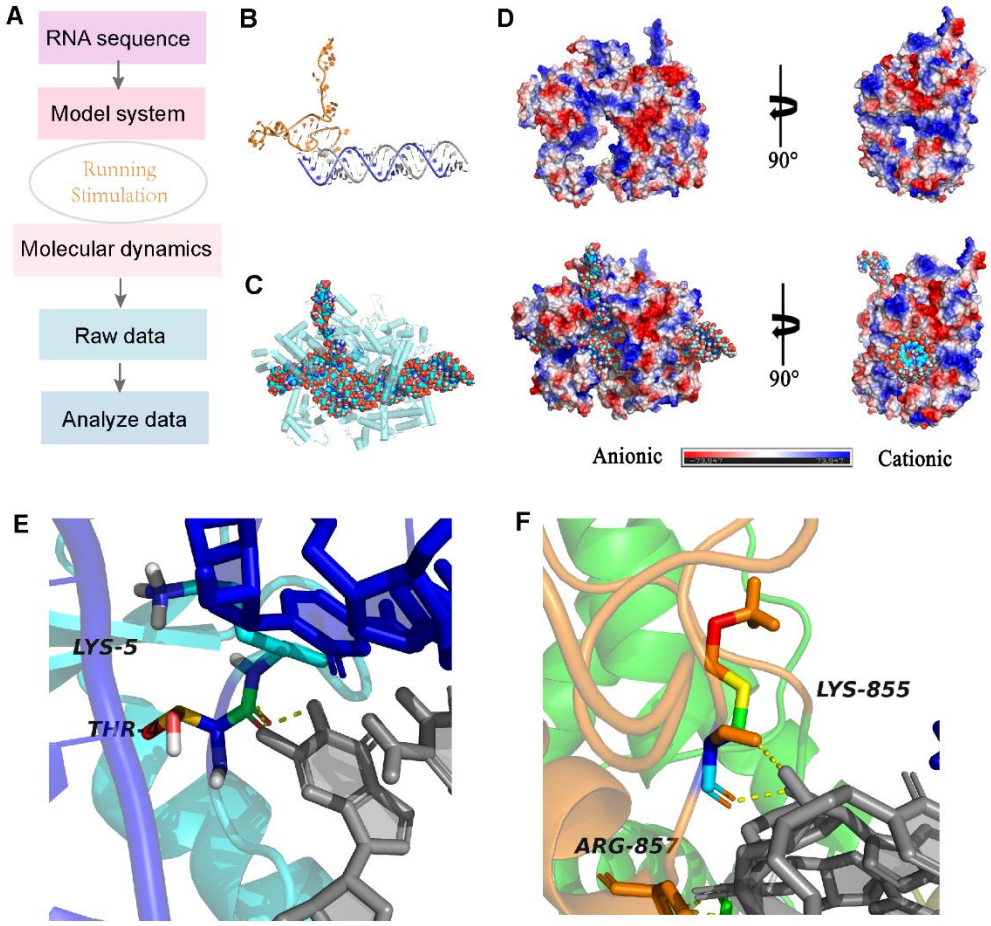

Figure S1. Analysis of the interaction between Cas13a and crRNA14. (**A**) A flowchart depicting the *in silico* assessment process used to identify suitable crRNA candidates. (**B**) 3D structure of the crRNA14-IDH1$_{mut}$ duplex. IDH1$_{mut}$ is in blue. (**C**) Van der Waals Surface of the crRNA14-IDH1$_{mut}$ duplex. (**D**)

Electrostatic binding surface analysis indicating that the negatively charged surface of crRNA14 matches well with the positively charged region in the catalytic groove of Cas13a. (**E**) Partially enlarged details of the hydrogen-bond interactions of Cas13a with the bases in the 16–29-bp segment of RNA14. (**F**) Partially enlarged details of the hydrogen-bond interactions of Cas13a with the bases in the 51–65-bp segment of RNA14.

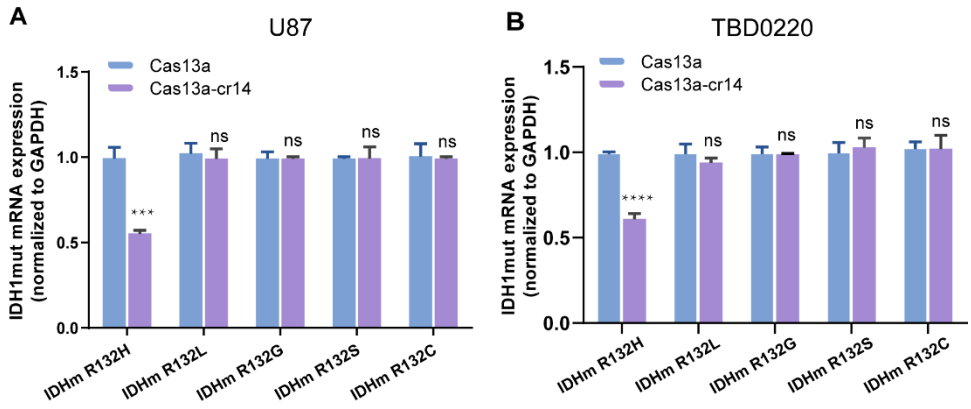

Figure S2. Confirmation of the efficiency of this strategy. (**A** and **B**) qRT-PCR analysis to examine the target mRNA level in U87 and TBD0220 cells. Data were analyzed by unpaired t-test (n = 3; mean ± SEM). ns represents $p > 0.05$. ***$P < 0.001$, ****$P < 0.0001$.

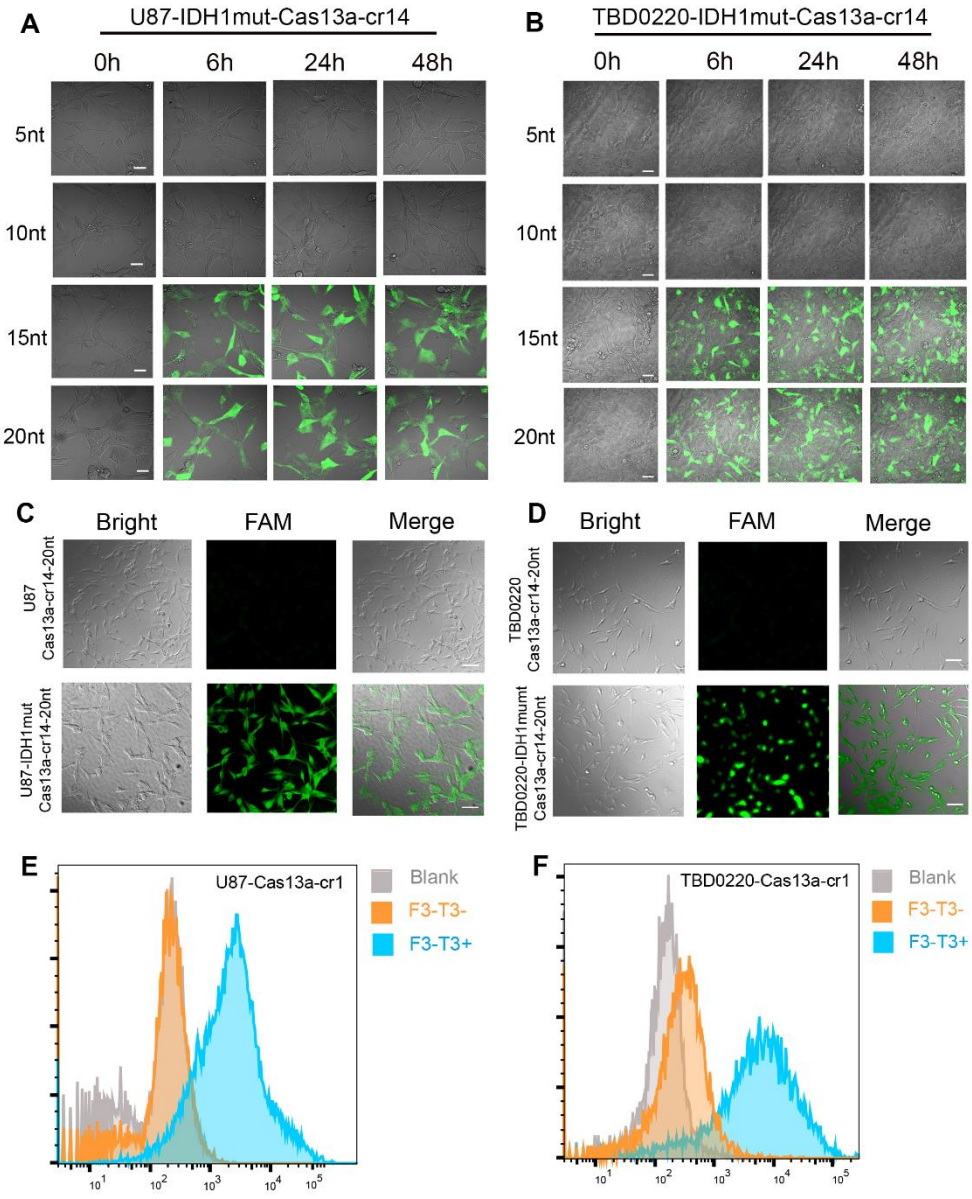

Figure S3. Validation of the efficiency of Cas13a-based reporter system. (**A** and **B**) Fluorescence microscopy images of FAM disruption in U87- and TBD0220-IDH1mut-Cas13a-crRNA14 cells treated with various reporter RNAs. Scale bar = 50μm. (**C**) Fluorescence microscopy images of FAM disruption in U87- and U87-IDH1$_{mut}$-Cas13a-crRNA14 cells treated with the reporter RNA. Scale bar = 100 μm. (**D**) Fluorescence microscopy images of FAM disruption in TBD0220- and TBD0220-IDH1$_{mut}$-Cas13a-crRNA14 cells treated with the reporter RNA.

Scale bar = 100 μm. (**E** and **F**) Analysis of the Cas13a-based reporter system in U87 and TBD0220 cells overexpressing F3-T3 gene chimera using flow cytometry.

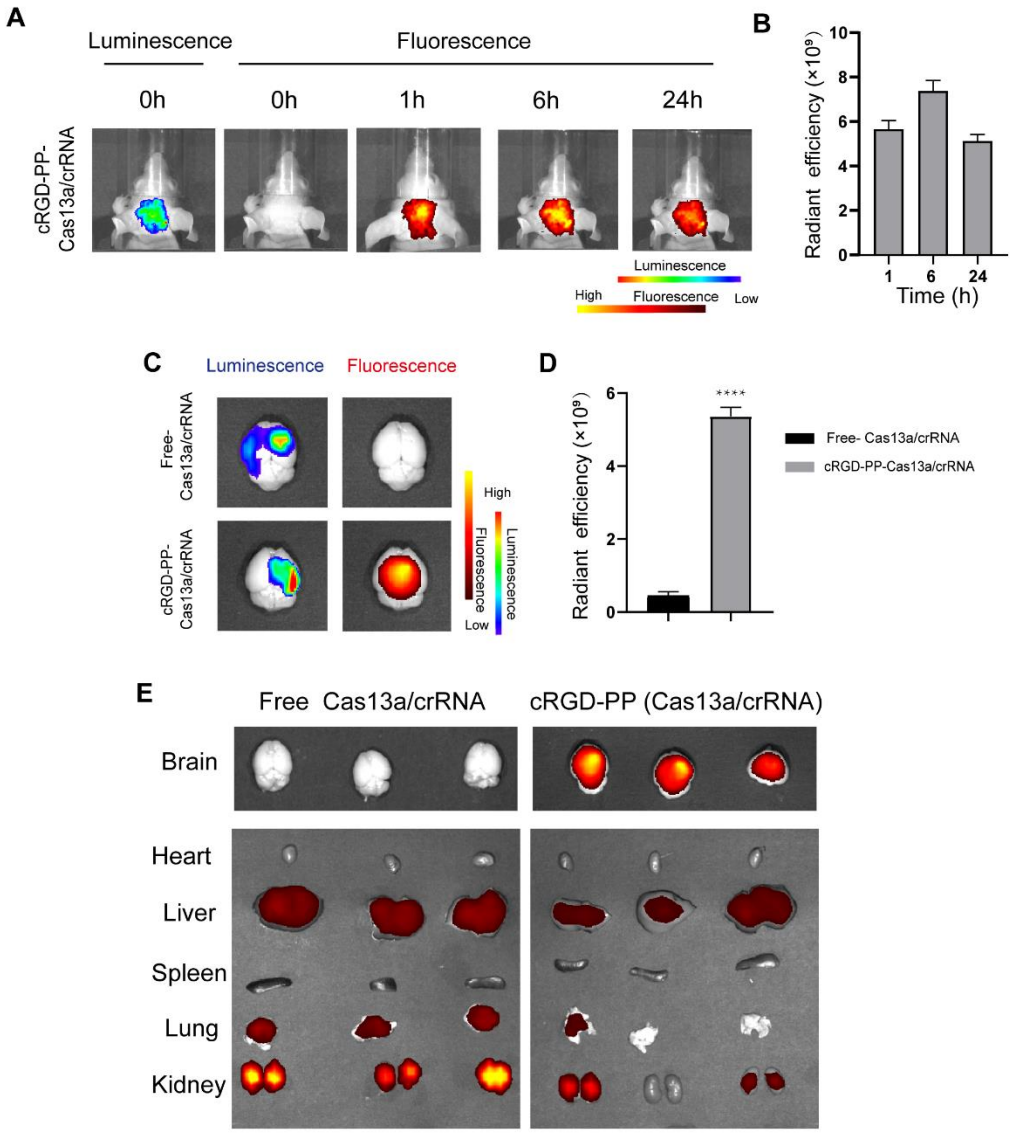

Figure S4. In vivo BBB penetration. (**A**) Real-time fluorescence tracking of TOTO-3-nanoparticles in the brain region of TBD0220-Luc-bearing mice (n = 3). (**B**) Statistical analysis of in vivo fluorescence images. (**C)** Representative ex vivo bioluminescence and fluorescence images of brains collected at 24

hours post-injection. (**D**) Ex vivo fluorescent images for statistical analysis. Data were analyzed by unpaired t-test (n = 3; mean ± SEM). ****P < 0.0001. (**E**) Ex vivo fluorescence images of the mouse brain and visceral organs after intravenous injection of cRGD-PP(Cas13a/crRNA) nanocapsules or controls.

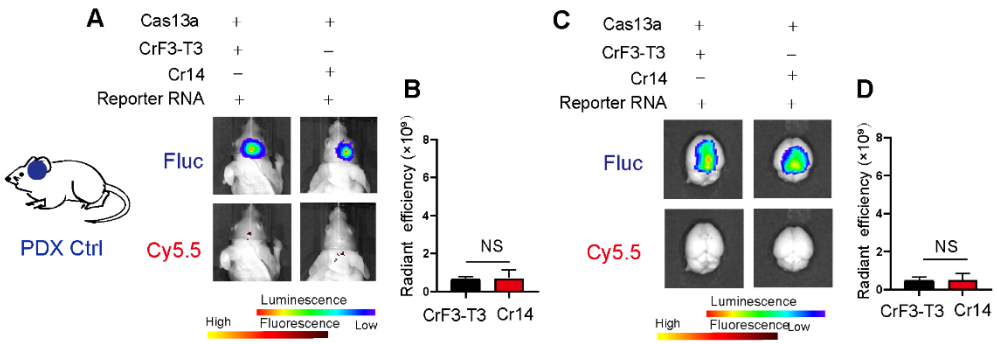

Figure S5. The sensitivity and accuracy of Cas13a-based detection system in vivo diagnosis. (**A**) Representative images of in vivo fluorescence and bioluminescence assays following the injection of cRGD-PEI-PBLG/pDNA/reporter RNA complex in mice without IDH1mut tumors. (**B**) Statistical analysis of in vivo fluorescence images. Data were analyzed by unpaired t-test (n = 3; mean ± SEM). ns represents p > 0.05. (**C**) In vitro fluorescence and bioluminescence images of mice brain sections following the cRGD-PEI-PBLG/pDNA/reporter RNA complex injection in mice without IDH1mut tumors via tail vein injection. (**D**) Ex vivo fluorescent images for statistical analysis. Data were analyzed by unpaired t-test (n = 3; mean ± SEM). ns represents p > 0.05.